

## **Ice Crystal Concentration in Midlatitude Cirrus Clouds: In Situ Measurements with the Balloonborne Hydrometeor Videosonde (HYVIS)**

**Narihiro ORIKASA, Masataka MURAKAMI**

*Meteorological Research Institute, Tsukuba, Japan*

**and**

**Andrew J. HEYMSFIELD**

*National Center for Atmospheric Research, Boulder, Colorado, USA*

*(Manuscript received 19 January 2012, in final form 22 November 2012)*

### **Abstract**

This study reports on the concentration of ice crystals measured in midlatitude cirrus clouds by a balloonborne hydrometeor videosonde (HYVIS), which has the advantage of measuring small ice crystals in the size range of 10–100  $\mu\text{m}$  more reliably. The cirrus clouds were generally associated with warm or stationary fronts of synoptic-scale lows. The microphysical dataset consisted of 37 launches from Tsukuba, Japan, during the observation period 1994–2007. On the basis of the comparison with concurrent data by other airborne instruments in the laboratory, the ice crystal concentrations can be measured by the HYVIS with an uncertainty factor of 2–3, although significant uncertainties are still included in the size range 10–30  $\mu\text{m}$ . The reliability of the measured concentrations is supported by the observed size spectra of the dataset in this study and the simulated total concentrations of ice particles with a parcel model.

Vertical profiles of size distributions of cirrus cloud ice crystals were obtained for clouds with top temperatures ranging from  $-33^{\circ}$  to  $-72^{\circ}\text{C}$  and base temperatures from  $-3^{\circ}$  to  $-49^{\circ}\text{C}$ . Ice crystal concentrations varied approximately from the order of  $10^{-1}$  to  $10^2 \text{ L}^{-1}$ . Median ice crystal concentrations were typically several tens per liter regardless of temperature or their vertical location. While the concentrations were sometimes the highest near the cloud top, some clouds had their maximum concentration near the cloud base. As ice particles near the cloud base were usually in sublimation zones, it is suggested that crystal breakup through the sublimation process enhanced the concentrations in some cases.

There was a large difference between the measured concentrations and simulated ones in earlier modeling studies of cirrus cloud formation that treated the ice crystal generation process through homogeneous ice nucleation of aqueous solution droplets, although the measured ones are probably affected by other physical processes such as secondary ice formation and gravitational sedimentation and turbulent mixing of ice particles after the initial cloud formation. Furthermore, a strong temperature dependence expected from heterogeneous ice nucleation formulas at relatively warm temperatures ( $> -25^{\circ}\text{C}$ ) was not found over all temperature ranges. Some implications for ice nucleation mechanisms in cirrus clouds in comparison with recent modeling studies involving heterogeneous ice nucleation at temperatures below  $-40^{\circ}\text{C}$  are briefly discussed.

**Keywords** cirrus cloud; ice crystal concentration; ice nucleation; balloonborne observation

### **1. Introduction**

Cirrus clouds, which occur over globally widespread areas, play an important role in the earth's radiation budget (Liou 1986). To understand their radiative properties, it is critical to know the size

---

Corresponding author and present affiliation: Narihiro Orikasa, Sendai District Meteorological Observatory, 1-3-15 Gorin, Miyagino-ku, Sendai, Miyagi 983-0842, Japan.  
E-mail: norikasa@met.kishou.go.jp  
©2013, Meteorological Society of Japan

distributions within these clouds and measure of their radiatively effective size (Stephens et al. 1990), as well as crystal shape (Mishchenko et al. 1996).

This study focuses on an examination of the concentrations of ice crystals in cirrus clouds, a microphysical variable of cirrus clouds that has been difficult to quantify in the past. While the number concentrations seem to have no direct link with the radiative properties of cirrus clouds, given an ice water content as measured from an aircraft or inferred from radar measurements, the concentrations and size distributions affect the “effective diameter” for cloud extinction, extinction coefficient, and cloud optical depth.

Airborne impactors (e.g., replicators, video ice particle samplers) have been used to quantify the concentrations of small ice particles in cirrus (e.g., Hallett 1976; Heymsfield and McFarquhar 1996; Schmitt and Heymsfield 2009). Measurements of ice crystal concentrations from airborne impactors can be unreliable because the larger crystals can breakup on their impactations at high speeds attained by an aircraft. Furthermore, the efficiencies at which impactors collect small ice particles have not been fully characterized either experimentally or numerically. The cloudscope developed by the Desert Research Institute (Schmitt and Arnott 1999), which is also an airborne cloud probe and has been used for detecting particles ranging from 3 to 400  $\mu\text{m}$ , has a feature of heating the microscope objective to prevent buildup of ice particles. Because it is difficult to estimate the geometry of the cloudscope, the collection efficiency for ice particles has not been intensively studied.

The cloud particle imager (CPI) probe developed by SPEC Inc., provides high-quality digital images for particles  $> 10 \mu\text{m}$  in diameter, and no airspeed correction is needed for most research aircraft (up to  $200 \text{ m s}^{-1}$ ) because of the fast electronic response time of the pulsed illumination and the CCD camera (Lawson et al. 1998a, 1998b), which is one of the main advantages. Lawson et al. (2001) reports a few methodologies to calculate particle concentrations; however, the sample volume for small particles ( $< 20 \mu\text{m}$ ) may still need to be investigated because of uncertainty in the detection threshold level of the CPI particle detection system, which directly affects its counting efficiency. In a recent study by Connolly et al. (2007), the errors in particle sizing and definition of the depth of field were assessed to propose a correction algorithm for particle size distributions measured with the CPI. The 2D-S (Stereo) probe, recently developed by SPEC Inc., is an optical array imaging instrument

utilizing two laser beams with a newer technology that supports high-resolution ( $10 \mu\text{m}$ ) and fast-time response (Lawson et al. 2006); resizing of out-of-focus images and counting efficiency for small particles ( $< 100 \mu\text{m}$ ) are significantly improved over older optical array probes. The effects of ice particle shattering on the arm tips for the 2D-S measurements need to be investigated in a comprehensive manner, even when the interarrival time algorithm for a particle appears to be more effective in mitigating the shattering effect than the modified probe tips (Lawson 2011).

The Particle Measuring System (PMS) imaging probes have been frequently used for measuring ice crystal size distributions. The PMS two-dimensional cloud probe (2DC) can only obtain reliable estimates of the concentrations down to a size of approximately  $125 \mu\text{m}$  on the basis of an assessment of the probe's performance in the wind tunnel experiment (Strapp et al. 2001). For smaller ice particles, a forward scattering spectrometer probe (FSSP) has been used in a number of studies. However, estimates of the concentrations of the small particles are uncertain because larger crystals can contribute to the concentrations of the FSSP (Gardiner and Hallett 1985) and the optical scattering characteristics of the ice particles are not clearly known (Heymsfield and Platt 1984). On the other hand, studies show that the FSSP could make reliable measurements for some types of cirrus clouds, such as contrail cirrus, cirrus outflow from hurricane, or arctic cirrus, where quasi-spherical small crystals were dominantly found and few large crystals were present (e.g., Gayet et al. 1996; Lawson et al. 2001; Ivanova et al. 2001). However, as pointed out by Gayet et al., the FSSP measurements can be quite unreliable for accurate sizing and counting ice particles in natural cirrus with large nonspherical ice crystals or relatively broad size distributions. Field et al. (2003) evaluated the effect of ice particle shattering on the FSSP inlet by analyzing the interarrival times for ice crystals and showed that the ice crystal concentrations measured in midlatitude cirrus could be overestimated typically by a factor of about 2 (by as much as a factor of 5 in the worst case). This issue of ice shattering holds true for the standard arm tips or inlets of the other airborne in situ probes for detecting ice crystals, such as 2DC, 2D-S, cloud imaging probe (CIP), and cloud and aerosol spectrometer (CAS). The artifacts for optical imaging probes can be mostly corrected in some cases on the basis of the particle interarrival times (Field et al. 2006) or significantly mitigated by using modified tips (Korolev et al. 2011). However, a more comprehensive

study is required for quantifying the effect of shattering on airborne in situ measurements, which is expected to depend on multiple factors including particle size and type (density, habit), airspeed, angle of attack, probe geometries and depth of field, and cloud conditions.

Balloonborne instruments can have the ability to measure the concentrations of small ice particles as their strength because minimal crystal breakup occurs at their ascent speed and they are designed to have a minimum detection threshold of 5–10  $\mu\text{m}$ . The hydrometeor videosonde (HYVIS) (Murakami and Matsuo 1990; Orikasa and Murakami 1997) and the balloonborne ice crystal replicator (Miloshevich and Heymsfield 1997) are two types of balloonborne instruments for cirrus cloud microphysical measurements. However, for these instruments, the collection efficiency decreases to sizes below 10  $\mu\text{m}$ , so few tiny crystals are actually sampled. More importantly, detailed analysis of the collection efficiency is needed for the impactor-type instruments with different flow fields and sample inlet systems because the dependence of the collection efficiency on particle size might be strongly influenced by deviations from a simplified theoretical approach, as suggested by Miloshevich and Heymsfield (1997).

It is difficult to directly detect ice crystal nucleation in cirrus clouds; the observed properties of cirrus clouds do not describe the conditions at the time of crystal generation. In contrast, wave clouds enable us to observe successive stages in the ice nucleation process (Heymsfield and Miloshevich 1993). Aircraft measurements in orographic wave clouds have been used to investigate ice nucleation processes at low temperatures (over the range from  $-30^\circ$  to  $-56^\circ\text{C}$ ), and the results from wave cloud studies have been used to gain a better understanding of the ice formation and evolution processes in cirrus clouds (Heymsfield and Miloshevich 1993, 1995). The measurements were consistent with the scenario by numerical modeling that involves the formation and growth of haze particles and subsequent homogeneous freezing. Homogeneous ice nucleation was introduced as a means of explaining the presence of liquid water supercooled to  $-36^\circ\text{C}$  and its absence at temperatures below  $-36^\circ\text{C}$  (Sassen and Dodd 1988, 1989; Heymsfield and Sabin 1989). Jensen et al. (1998) also compared in situ measurements in wave clouds with numerical simulations. The observed peak ice crystal concentrations and peak relative humidities were consistent with the simulated values at moderate to high updraft velocities ( $1\text{--}4\text{ m s}^{-1}$ ) for wave clouds.

The rate of ice production by homogeneous nucleation depends strongly on the updraft velocities (DeMott et al. 1994). Because the vertical velocities in the wave clouds studied by these researchers were one or more meters per second, the homogeneous ice nucleation process is interpreted as a dominant ice nucleation mechanism within vigorous convection and updrafts of cirrus clouds.

DeMott et al. (1994) have studied the interplay of homogeneous versus heterogeneous ice nucleation processes in cirrus clouds conducting sensitivity studies with a Lagrangian parcel model and with a 2D version of a mesoscale cloud model (CSU/RAMS). They found that the cloud condensation nucleus (CCN) and ice nucleus (IN) profiles in the vertical (with temperature) have a profound effect on which ice nucleation mechanism is dominant. They also found that heterogeneous nucleation dominates when the updraft velocities are low, which corresponds to cirrus clouds associated with synoptic-scale ascent, and leads to relatively low ice crystal concentrations (of the order  $10\text{ to }100\text{ L}^{-1}$ ). With vigorous updrafts, homogeneous nucleation (freezing) of cloud and solution droplets dominates and leads to concentrations as large as several tens per cubic centimeter.

Box model studies (e.g., Gierens 2003) suggest that the suppression of homogeneous ice nucleation depends on environmental conditions (including updraft velocities) as well as the amount of heterogeneous ice nuclei. Within the framework of a 2-D nonhydrostatic model, the process of ice particle sedimentation, which is usually not implemented in box models, can be incorporated for the investigation of the effect of both ice nucleation mechanisms on the life cycle of cirrus clouds (Spichtinger and Gierens 2009). Such recent modeling studies introduce new insights and implications on the interplay of nucleation mechanisms in natural cirrus clouds.

In this study, we report on the concentrations of ice crystals measured by the HYVIS in cirrus clouds generally associated with warm or stationary fronts of synoptic-scale lows, basic to the study of cirrus cloud properties and ice nucleation processes in the atmosphere. From these observations, we speculate on some aspects of the nucleation processes.

## 2. Instruments and cirrus particle data

The HYVIS collects particles larger than about 10  $\mu\text{m}$  on a silicone-oil-coated film (35-mm wide, transparent leader film; Fuji Photo Film Co.); a new section of film is drawn out of a magazine at intervals of about 10 s. The particles are imaged by two video cameras (Sony

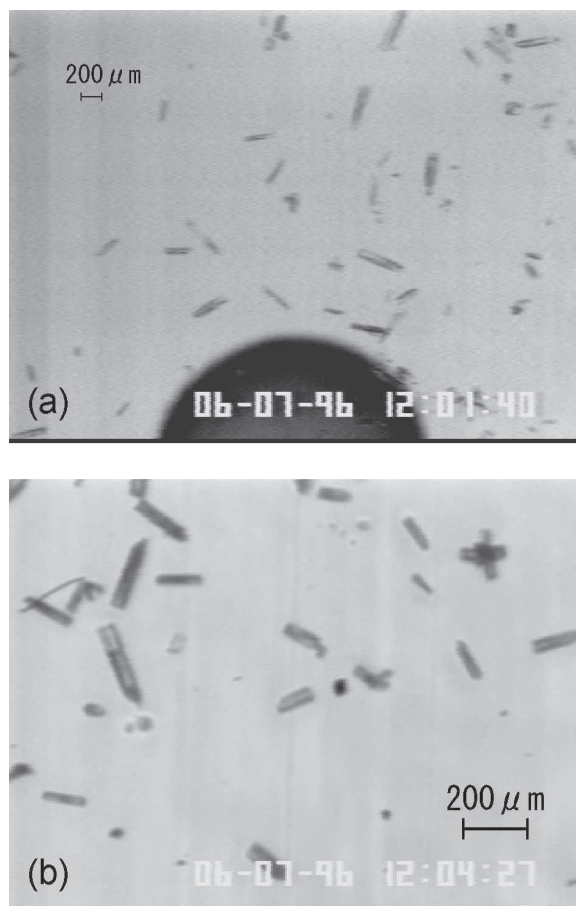


Fig. 1. HYVIS images taken with a close-up camera (top) and a microscopic camera (bottom).

HVM-52H) with different magnifications; they are referred to as close-up camera and microscopic camera, and the areas of each image are  $5.48 \text{ mm} \times 4.04 \text{ mm}$  and  $1.79 \text{ mm} \times 1.32 \text{ mm}$ , respectively. To increase the sample volume, the HYVIS has a small suction fan (Micronel V484M) that draws hydrometeors into a particle inlet with no effects on particle breakup; the flow velocity reaches approximately  $12 \text{ m s}^{-1}$ , corresponding to a flow rate of about  $1 \text{ L s}^{-1}$ . Examples of HYVIS images with two video cameras are presented in Fig. 1. The images are transmitted in realtime via a 1687-MHz microwave to a ground station. The HYVIS sample volume and collection efficiency for the small particles have been quantified by both wind tunnel experiments and theoretical studies based on impaction experiments by Ranz and Wong (1952). According to these methods, the HYVIS sample volume corresponds to  $0.25 \text{ L s}^{-1}$  for a closeup image or  $0.028 \text{ L s}^{-1}$  for the microscopic image at a

flow speed of  $12 \text{ m s}^{-1}$ , and the collection efficiency was considered to be nearly unity for all particles larger than  $10 \mu\text{m}$  (Orikasa and Murakami 1997).

To confirm the actual collection efficiency, we have recently conducted calibration experiments in our laboratory with small particles by comparing with the concurrent data of other instruments. The Appendix describes such comparison and uncertainty in the HYVIS measurements. Although currently there is neither a standard instrument nor a standard technique for number concentration measurements of cloud particles, the calibration experiments here should be regarded as a reference. We estimated from the comparison that the number concentrations of ice particles in the size range  $10\text{--}100 \mu\text{m}$  measured with the HYVIS would be accurate within only a factor of 2 to 3 partly owing to the uneven distribution of actually collected particles on the suction area. In contrast to the HYVIS, large uncertainties still remain in the

number concentrations of particles smaller than  $50\text{ }\mu\text{m}$  for currently available airborne instruments owing to errors caused by ice particle shattering and sample volume uncertainties (Baumgardner et al. 2012).

On the basis of the theoretical approach, the collection efficiency (*CE*) of the HYVIS for all particles larger than  $10\text{ }\mu\text{m}$  is determined to be unity (Orikasa and Murakami 1997). The comparison with other microphysical instruments (see Appendix) suggested that the *CE* of the HYVIS had the uncertainty within a factor of 2 to 3 for  $10\text{--}30\text{ }\mu\text{m}$  particles and with a factor less than 2 for particles larger than  $30\text{ }\mu\text{m}$ . In this study we assumed the *CE* was unity for all particles actually collected because further data are still required to establish the correction of *CE* as a function of particle size.

Figure 2 shows examples of size distributions measured by the HYVIS. Only the size distributions near the cloud top are shown because most ice crystals in this region are likely to be nucleated in this region and less affected from other regions. For some distributions in Fig. 2, the concentration falls off rapidly for sizes smaller than  $50\text{ }\mu\text{m}$ , while particles are fed into the smallest bin in most of the size distributions. The HYVIS measurements also show broad size distributions with gentle slopes, even at cold temperature ( $-50^{\circ}\text{C}$  to  $-70^{\circ}\text{C}$ ), where the growth rate of ice crystals is significantly lower than that at a warmer temperature ( $> -40^{\circ}\text{C}$ ) under the same ice supersaturation. The gentle slopes in smaller size ranges suggest that no intensive ice nucleation could occur.

In such a case where tiny ice particles are dominant in the size range from a few microns to  $10\text{ }\mu\text{m}$ , the HYVIS measurements show large errors in the total number concentrations. Although this is a limitation for the instrument, it is unlikely that the measured concentrations in the synoptically generated cirrus in our dataset would cause a systematic bias to the profiles of ice particle populations, which is inferred from the uncertainty of the *CE* of the HYVIS, the measured size distributions of ice particles, and the comparison between the measured and simulated number concentrations mentioned in Section 4.

For the image processing of the HYVIS measurements, the particle size (maximum dimension), concentration, and crystal habit of cirrus cloud particles were derived from each image, which was manually determined and processed. Because the HYVIS images were recorded as a motion picture, separation of overlapping particles or determination of ice crystal breakup during impaction on the film by visual analysis is facilitated, which has been inferred

from frame-by-frame analysis. The fragmentation by breakup upon impaction with the HYVIS was observed to be about 5% of the total counts at most in our dataset, and such particles were excluded in order to avoid any artificial concentrations. In this study, only the maximum dimension was recorded for the size distributions of ice particles. Automatic image processing software enables further analysis to acquire useful information such as the aspect ratio and area ratio of each particle or the relationship between its dimensions and cross-sectional area. We will report this result in the future study.

Relative humidity (RH) and temperature profiles were simultaneously measured with a rawinsonde (JMA model RS2-91; Meisei Electric Co.) whose signals were transmitted on a 1673-MHz microwave carrier. Since the 2004 campaigns, a GPS sonde (Model RS-01G; Meisei Electric Co.) was used to measure meteorological parameters, whose humidity sensor has basically the same specification as that of the RS2-91 rawinsonde. The RH sensor uses the principle of a thin-film capacitive method; the same principle is used by the Vaisala RS80-A sensor. At cold temperatures, this type of RH sensor exhibits a dry-bias error that increases significantly with decreasing temperature below  $-30^{\circ}\text{C}$  (Miloshevich et al. 2001). Because the magnitude of the measurement error depends highly on the type of sensor and a correction algorithm for our sensor is yet to be developed, we presented the uncorrected data of RH measurements in this study.

The cirrus cloud microphysical dataset was collected by the HYVIS during the period 1994–2007. We have successfully acquired and analyzed the imagery for 37 launches of the HYVIS, consisting of about 4600 video images of ice particles in cirrus clouds, in 1994–1999 as part of the Japanese Cloud and Climate Study (JACCS) field program and in 2003–2007 as post-JACCS field campaigns. The JACCS cirrus experiment was conducted from Tsukuba ( $36.0^{\circ}\text{N}$ ,  $140.1^{\circ}\text{E}$ ), Japan. The ground-based observational system consisted of a special sonde (HYVIS + radiation sonde) system, a cloud lidar, a windprofiler, and various types of spectroradiometers (Asano et al. 1997). In the post-JACCS campaigns, the limited instruments, lidar and radiometers as well as the HYVIS, were operated.

We have obtained the observational dataset of cirrus clouds generally associated with a midlatitude warm front of a synoptic-scale low, a stationary (Baiu) front, or a strong jet stream during spring to early summer (from March to July, mostly in May and in June). The



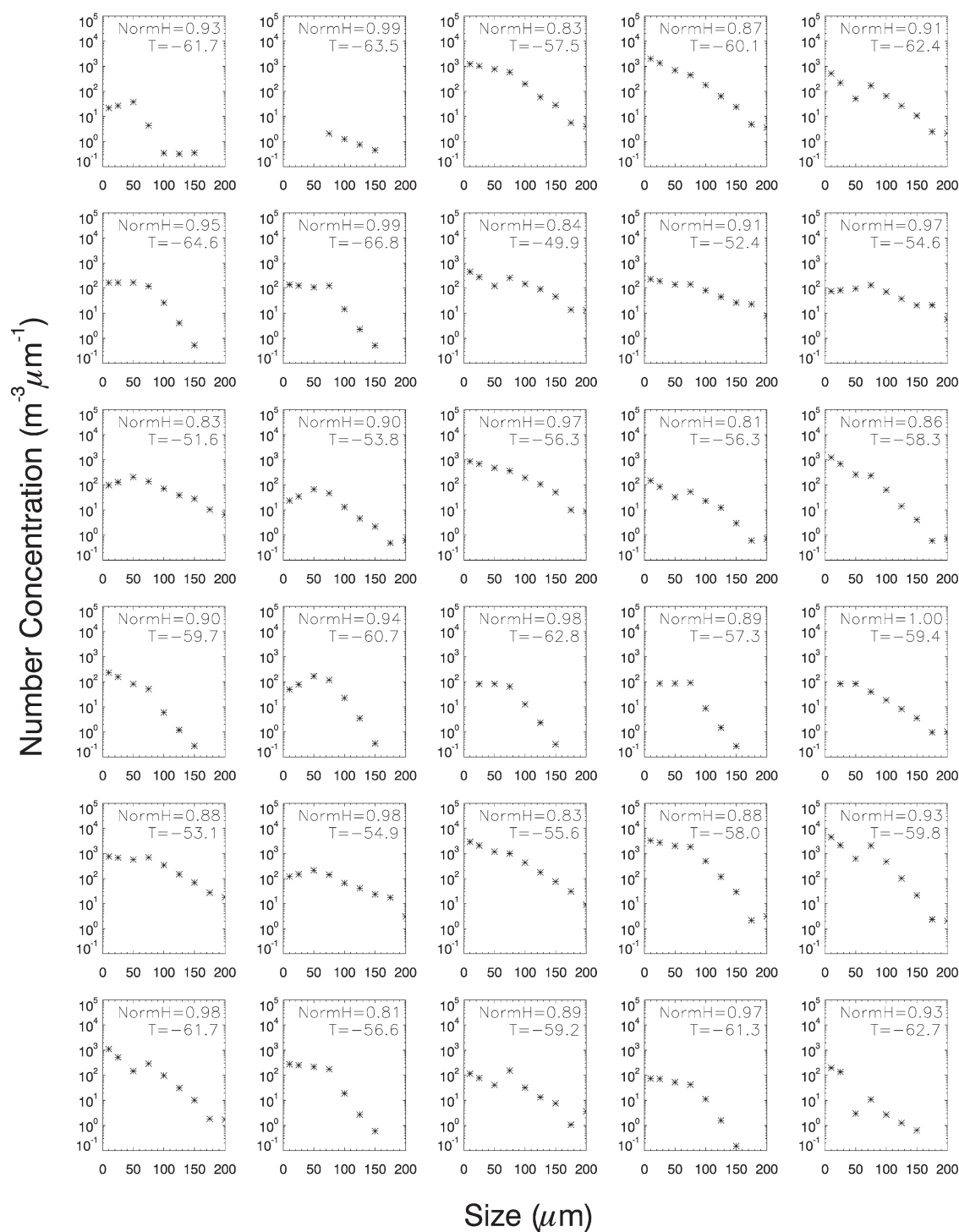


Fig. 2. Size spectra up to  $200 \mu\text{m}$  from HYVIS measurements in cloud top regions ( $\text{NormH} > 0.8$ ). Normalized height and ambient temperature ( $^{\circ}\text{C}$ ) in upper right corner of each panel. Each panel represents a size spectrum averaged over a 250-m height interval.

dataset contained herein was obtained from mostly cirrostratus and/or cirrus, identified by a trained meteorological observer on the basis of a cloud atlas (WMO 1975), while in about 20% of all cases, cirrostratus was linked together with altostratus (no water droplets from the HYVIS imagery) so that it was difficult to identify the line between two types of cloud. Although the definition of a cirrus cloud needs to be carefully considered in order to determine its climatology (Sassen and Campbell 2001), we consider it reasonable to regard all our data as cirrus clouds on the basis of comparison with other datasets (Dowling and Radke 1990). Besides, neither case of precipitation nor anvil clouds from deep convection was included in the dataset studied here. There were no in situ aircraft measurements and cloud radar data available.

### 3. Results of ice crystal concentration data analysis

Vertical profiles of ice crystal size distributions in cirrus clouds were obtained for 37 cases observed by the HYVIS. Hereafter, the minimum and maximum altitudes where ice particles were detected are referred to as cloud base and cloud top, respectively. Therefore, ice saturation and/or supersaturation could not be assured inside the clouds presented here. Cloud depths (actual vertical distances) varied from 1.1 to 8.8 km (average: 4.8 km) with cloud top heights ranging from 8.2 to 14.1 km and base heights from 2.7 to 11.9 km. Cloud top temperatures ranged from  $-33^{\circ}$  to  $-72^{\circ}\text{C}$ , while base temperatures from  $-3^{\circ}$  to  $-49^{\circ}\text{C}$ .

The results of vertical distributions of total ice crystal concentrations are shown in Fig. 3, where the ice crystal concentrations are plotted as a function of normalized height ( $NormH$ ) such that cirrus cloud base height = 0 and cloud top height = 1 in a relative sense in each case. These plots are classified according to the cloud top temperatures, as shown. Although the dataset had fewer cases with cloud top temperatures above  $-55^{\circ}\text{C}$ , ice crystal concentrations varied from the order  $10^{-1}$  to  $10^2 \text{ L}^{-1}$ . The concentrations of ice crystals larger than  $30 \mu\text{m}$  are also shown as the median value (dashed line) in Fig. 3. There was little difference between the two concentrations, including and excluding ice crystals in the size range of  $10\text{--}30 \mu\text{m}$ .

The number concentrations of ice crystals were sometimes the highest near the cloud top; however, their trend of increasing with distance below the cloud top is shown in Fig. 3. In contrast, the ice crystal concentrations decreased in the vicinity of the cloud base owing to sublimation, although aggregation could occur for some of the clouds. To examine where the

maximum ice crystal concentration occurred in the vertical distributions of the ice clouds, Fig. 4 shows both geometrical distances from the cloud top and cloud normalized heights where the maximum concentration occurred as a function of cloud depth. The maximum concentrations occurred at various heights inside cirrus clouds; about 35% of all cases had the maximum concentration near the cloud top ( $NormH \geq 0.8$ ), 16% near the cloud base ( $NormH < 0.2$ ), and 49% around the middle of clouds ( $0.2 \leq NormH < 0.8$ ). There was no correlation between the cloud depth and normalized height or distance below the cloud top with the maximum concentrations. However, which stage of cloud evolution in cirrus clouds the HYVIS penetrated should be considered in order to further understand the vertical microphysical structure, which we were unable to determine owing to poor coordination with other observation devices in both time and vertical columns.

RH profiles are one of the crucial factors affecting the size distributions of ice crystals. Figure 5 shows the vertical distributions of the RH with respect to ice observed within the cirrus clouds. Clearly, the RH rapidly decreased with decreasing height in the cloud regions,  $NormH < 0.1$ , although there would have been significant underestimation in the rawinsonde RH measurements at low temperatures, as mentioned in Section 2.

Ice crystal habits detected from the HYVIS imagery were examined to infer whether some of the enhanced concentrations near the cloud base or the sublimation zone ( $NormH < 0.1$ ) as shown in Fig. 4 could have been due to the breakup of rosettes; Gow (1965) reports that single bullets result from the breakup of rosettes from sublimation. Ice crystals detected by the HYVIS measurements were classified visually according to their crystal habits. The single bullet type of ice crystals was dominant, as shown in Fig. 6. In this figure, the occurrence frequency of bullet rosettes decreased with decreasing height. Also shown is the tendency toward an increase in the frequency of single bullet or column near the cloud base. These results together with the RH profiles are consistent with the scenario that single bullets are formed as a result of the breakup of bullet rosettes in sublimation regions (Gow 1965). The breakup of bullet rosettes may be attributed to one of the major factors that produced the maximum concentrations even near the cloud base. The laboratory study by Dong et al. (1994), where ice particle breakup during evaporation produced secondary ice crystals, could also support the breakup of bullet rosettes under subsaturated conditions in cirrus

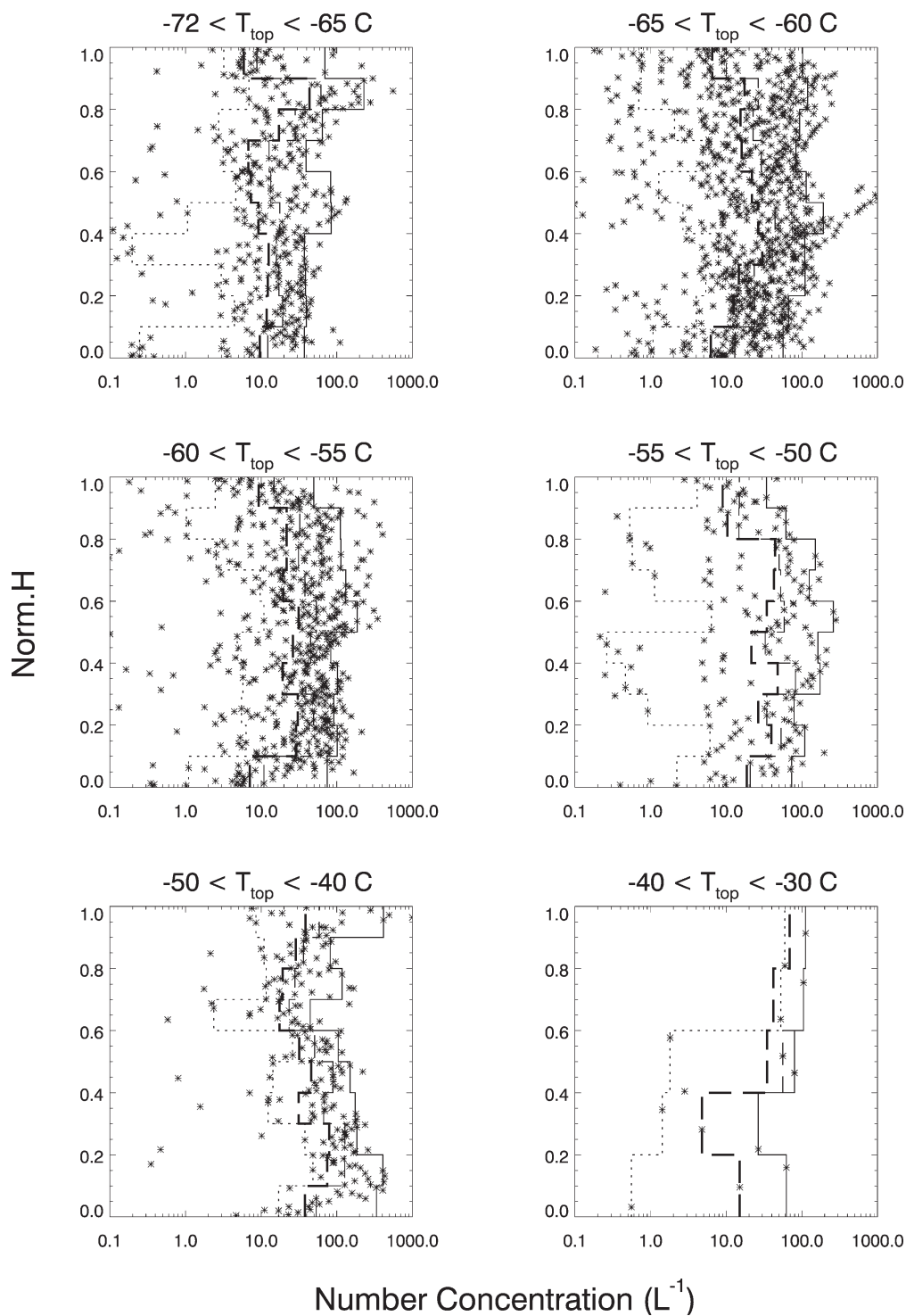


Fig. 3. Vertical distributions of ice crystal concentration observed in this study as a function of normalized height (NormH), sorted by cloud top temperature; asterisk indicates each measurement of the HYVIS. In each panel, the dotted line, thin dashed line, and solid line indicate the 10<sup>th</sup>, 50<sup>th</sup>, and 90<sup>th</sup> percentiles of concentrations of particles larger than  $10 \mu m$ , respectively, whereas the thick dashed line indicates the 50<sup>th</sup> percentile of concentrations of particles larger than  $30 \mu m$ .



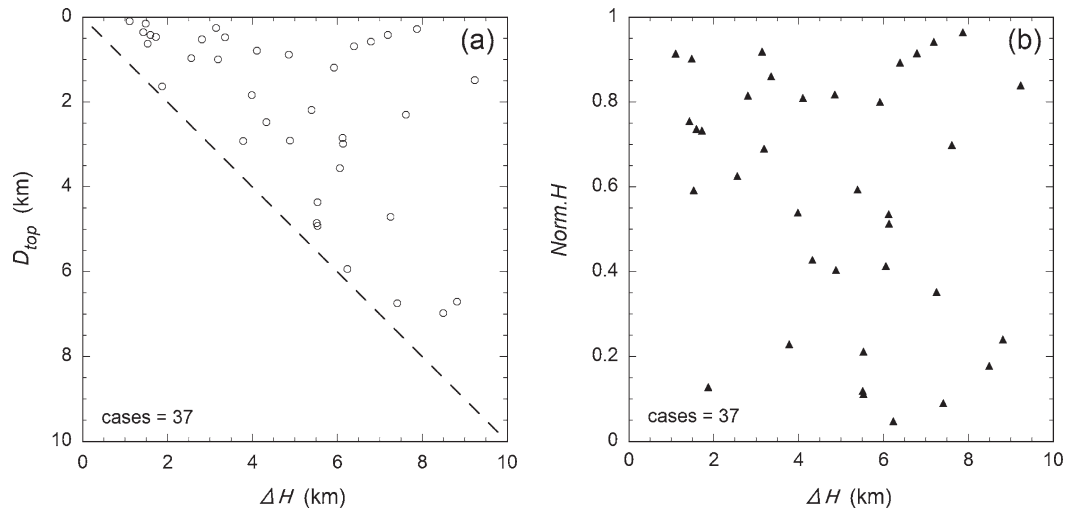


Fig. 4. Geometrical distance from the cloud top ( $D_{top}$ : open circles, panel a) and normalized height ( $Norm.H$ : filled triangles, panel b) in each case where the maximum ice crystal concentration occurred as a function of cloud depth ( $\Delta H$ ). Dashed line in the panel (a) corresponds to cloud base ( $\Delta H = D_{top}$ ).

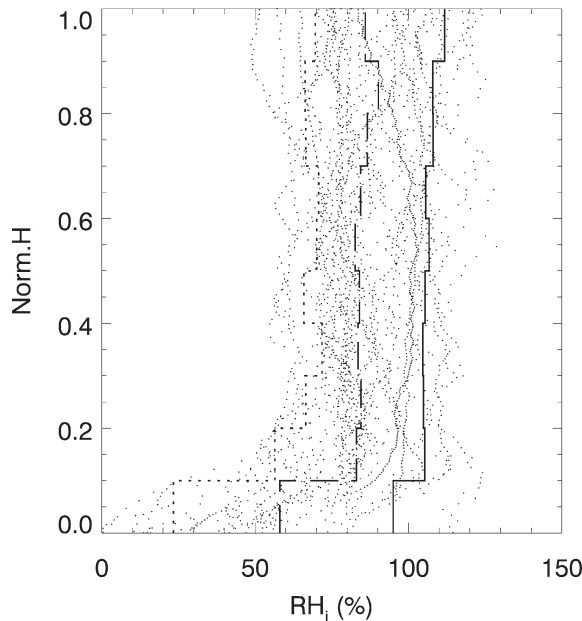


Fig. 5. Profiles of relative humidity with respect to ice as a function of  $Norm.H$  within the cirrus clouds observed in this study. The dotted line, dashed line, and solid line indicate the 10<sup>th</sup>, 50<sup>th</sup>, and 90<sup>th</sup> percentiles, respectively.

clouds.

The vertical profiles of thermodynamic stability might provide some indication of whether the cirrus crystals were produced in large-scale ascent, with vertical velocities of the order of  $1\text{--}10\text{ cm s}^{-1}$ , or in smaller-scale convective cells with vertical velocities of the order of  $100\text{ cm s}^{-1}$ , as shown in Fig. 7. Stability was examined by calculating the lapse rate ( $\Gamma_{PTE}$ ) of equivalent potential temperature from every 8-s measurement of RH and temperature for each cloud sublayer including 100 m above and below a reported level of rawinsonde measurements. A neutral stability refers to the condition where  $\Gamma_{PTE}$  in the figure is near zero. The thermodynamic conditions in the upper half of the clouds tend to be neutral with respect to equivalent potential temperature, except the regions very near the cloud top. Meanwhile, the stability in the lower half of the clouds, except the cloud bottom regions, showed a discernible tendency to increase with decreasing height. This is determined primarily by the structure of a warm front. Sublimation and associated local cooling near the cloud base would have produced relatively large lapse rates near the cloud base.

To obtain smooth (or representative) size distributions of ice crystals, vertical averaging of the HYVIS data is usually taken over 250-m-thick cloud layers. To verify whether the vertical averaging affects the interpretations, we test several ways of averaging. The

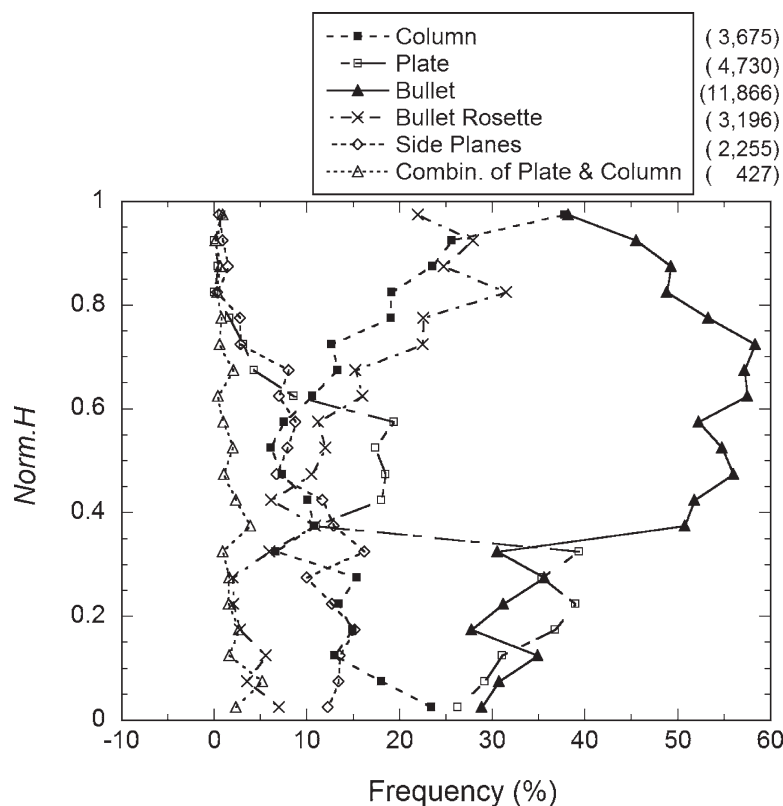


Fig. 6. Average appearance frequencies of ice crystal habits as a function of  $Norm.H$ . The number next to the legend represents the total count of ice crystals in each category analyzed from the high-magnification (microscopic) images in the HYVIS dataset.

vertical profile of the measured ice crystal concentrations can be resolved into fine intervals ( $\sim 10$  s) on the basis of the analysis of each video image, which corresponds to a vertical resolution of 40–140 m (average: 80 m), according to ascent rates (typically 6–8  $\text{m s}^{-1}$ ) of the HYVIS. (It takes about 5–15 min to penetrate a vertical column of cirrus.) Figure 8 provides the comparison of the maximum ice crystal concentrations with degraded vertical resolutions (250 m, 500 m, and 1 km); it displays distributions of the maximum concentration in the whole cloud region and four cloud regions partitioned by normalized height. The degradation of vertical resolution had a major impact on finding high concentrations in every case because its statistics consistently decreased with increasing vertical intervals and had no discernable effect on the concentrations among different vertical relative locations. It was shown in Fig. 8 that the vertical averaging over 250 m can be deemed acceptable to discuss the range of ice crystal concentrations in the vertical.

#### 4. Discussion and implications of HYVIS measurements

In this section, we first present the cirrus microphysical measurements from the other balloonborne ice crystal collector, the ice crystal replicator (Miloshevich and Heymsfield 1997), in order to obtain further support for the number concentrations measured by the HYVIS presented in section 3. Second, by comparing the HYVIS measurements and the recent results of cirrus modeling studies, some implications for ice nucleation mechanisms in cirrus clouds are discussed.

##### 4.1 Comparison with ice crystal replicator data

The microphysical data of the balloonborne ice crystal replicator presented here were collected on November 25, November 26, and December 5 in 1991 during the FIRE II experiment near Coffeyville, Kansas (Miloshevich and Heymsfield 1997). These data and the associated ice particle imagery have been

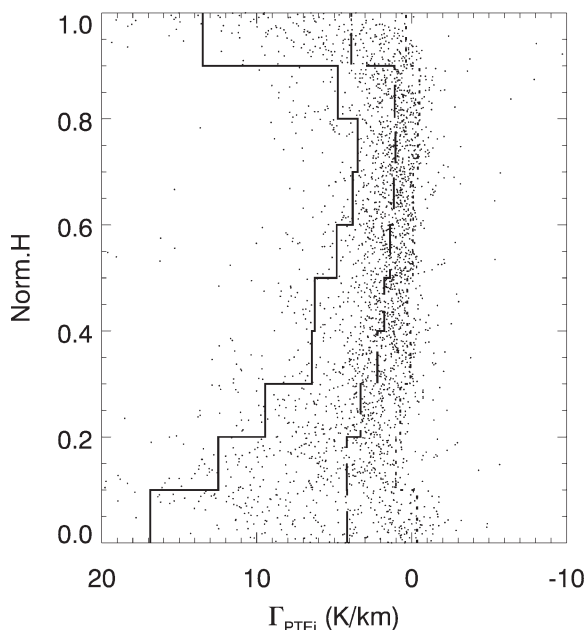


Fig. 7. Same as Fig. 5 but for thermodynamic stability profiles. Each point was derived from the lapse rates of equivalent potential temperature in each cloud sublayer including 100 m above and below a reported level from rawinsonde measurements.

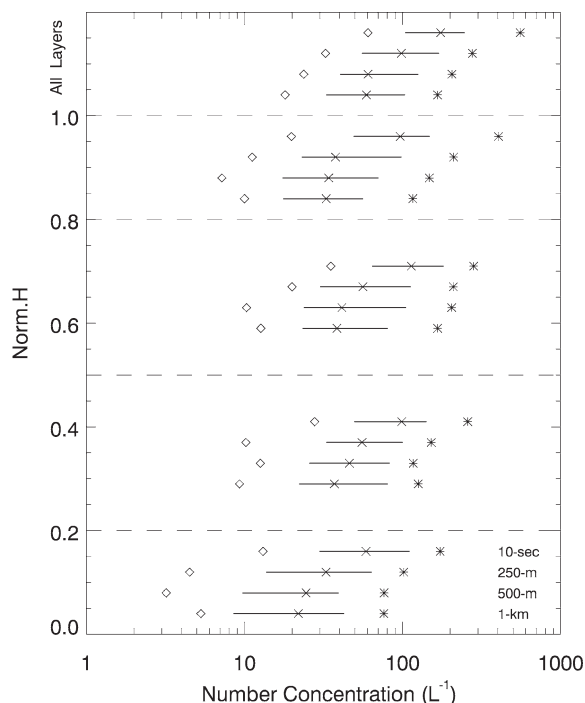


Fig. 8. Comparison of distributions of the maximum ice crystal concentrations measured with the HYVIS for different vertical resolutions. The whole cloud layer is partitioned into four cloud regions according to normalized height, as indicated by horizontal dashed lines. The distributions of the maximum concentration in terms of the whole layer are also shown at the top of the figure. The four distributions shown in each domain of the figure are for 10-s (average: 80 m), 250-m, 500-m, and 1-km vertical resolution in order from the top, respectively. Solid lines represent the run between the 25<sup>th</sup> and 75<sup>th</sup> percentiles of number distributions. Diamonds, crosses, and asterisks represent the 10<sup>th</sup>, 50<sup>th</sup>, and 90<sup>th</sup> percentiles, respectively.

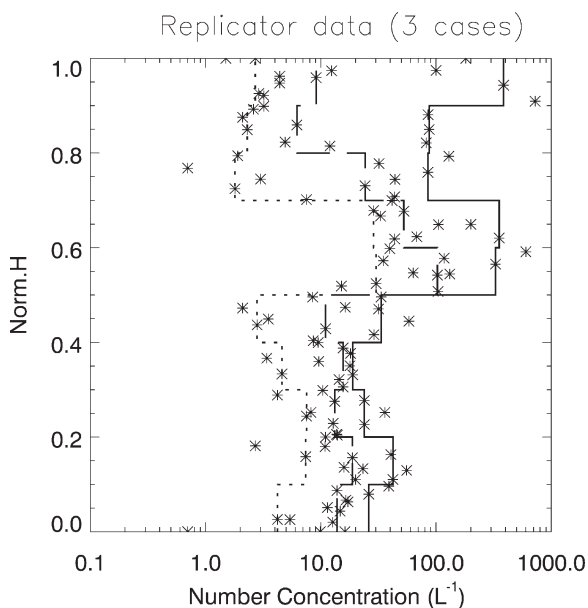


Fig. 9. Same as Fig. 3 but for the ice crystal concentrations from the balloonborne ice crystal replicator data during the FIREII experiment (courtesy of Larry Miloshevich).

reported in Miloshevich and Heymsfield (1997). These three cases had cloud top temperatures (altitude) of  $-56.9^{\circ}$  (10.41 km),  $-53.3^{\circ}$  (9.74 km), and  $-65.4^{\circ}$  C (12.63 km), respectively.

Similar to Fig. 3, for the HYVIS measurements, the vertical distribution of ice crystal concentrations are shown in Fig. 9. Although there were limited cases with replicator data, the ice crystal concentrations ranged from the order  $10^0$  to  $10^2$   $L^{-1}$ , which is similar to the results of the HYVIS measurements. The vertical distributions exhibited the highest ice crystal concentration in the middle of the cloud or near the cloud top and typically low concentration in the lower half of the cloud.

#### 4.2 Implications of ice crystal concentrations from HYVIS measurements

In the Cirrus Parcel Model Comparison (CPMC) Project (Lin et al. 2002), under the GEWEX Cloud System Study (GCSS) Working Group on Cirrus Cloud Systems (WG2), systematic efforts were directed toward assessing the understanding of ice crystal nucleation and evolution of microphysics in a closed air parcel by comparing with cirrus simulations using seven models. Although qualitative agreement has been found among the models for the simulations only with homogeneous nucleation, significant differences were reported in the comparison of predicted ice crystal concentrations. Lin et al. (2002) reported that some critical factors affected the predicted concentration, such as homogeneous ice nucleation rate, haze particle solution concentration, and growth rate of small ice crystals.

Ongoing laboratory studies in conjunction with modeling studies are becoming an important approach to improve our understanding of cirrus ice formation mechanisms (DeMott 2002, 2007). The laboratory results are useful for formulating the cirrus cloud processes in numerical models where many aspects are poorly understood and are not well-incorporated. To explore the relevance of ice crystal nucleation events in cirrus, we make qualitative comparisons between the HYVIS observations and previous cirrus modeling studies focused on homogeneous and heterogeneous ice nucleation. In the HYVIS dataset, we had no information of primary importance to ice crystal nucleation, including the updraft velocity and size spectra and chemical composition of both CCN and IN. Accordingly, our intention is to examine the range of possibilities on the ice nucleation process. For quantitative comparisons, such additional information from observations is required at the minimum to simulate cirrus formation, which is beyond the scope of this study.

As an example of the simulation of homogeneous ice nucleation, we perform sensitivity tests in this study by using the parcel model of Heymsfield and Miloshevich (1993). Although their model was not included in the study by Lin et al., the predicted ice crystal concentration was within the limits of differences among the seven models. The Lagrangian parcel model was run in a closed air parcel with prescribed, fixed updrafts, where no particle fallout was allowed (details in Heymsfield and Sabin 1989). Constant updraft velocities of 10, 50, and 100 cm s<sup>-1</sup> were used here as a sensitivity test for these simulations. The initial atmospheric environment (temperature, relative

humidity, and pressure) was set on the basis of standard atmosphere with subsaturated conditions with respect to water: 90% at -40°C, 70% at -60°C, and linearly interpolated relative humidities at temperatures between the two abovementioned temperatures. Although the physical and chemical properties of aqueous aerosols are fundamental information for homogeneous ice nucleation, the aerosol with one composition namely ammonium sulfate CCN was assumed, whose supersaturation spectrum was given by the power-law form ( $N_{CCN} = CS^k$ , where  $N_{CCN}$  (cm<sup>-3</sup>) is the total CCN concentration that is activated when a supersaturation with respect to water  $S$  (%) is achieved) with constants  $C$  (scaling factor, cm<sup>-3</sup>) and  $k$  (slope) of 100 and 0.5, respectively, and coincident observations of CCN narrow the uncertainties associated with this aspect. (Sensitivity tests on the CCN spectrum were given in Heymsfield and Miloshevich (1995); ice crystal concentrations can be substantially reduced if a limited number of effective CCN are available for homogeneous ice nucleation.) As pointed out by Lin et al. (2002), the deposition coefficient given in the modified vapor diffusion coefficient follows the findings of Fukuta and Walter (1970), which affects the growth rate of small ice crystals ( $< 10 \mu\text{m}$ ), and vapor depletion rate has a substantial impact on the resulting ice crystal concentration. Here we assumed 0.04 as the typical value of the deposition coefficient. Increasing this parameter to unity results in a decrease of  $\sim 1$  order of magnitude in the predicted concentration. Although the deposition coefficient is still an unknown parameter that may depend on environment variables such as temperature and supersaturation as well as size and surface structure of individual particles, the result of a recent laboratory experiment (Magee et al. 2006) supports the hypothesis of the numerical modeling study by Gierens et al. (2003) that the deposition coefficient is significantly smaller than unity, 0.01 or less in low-temperature conditions ( $< -40^\circ\text{C}$ ) with weak updrafts relevant to typical cirrus clouds.

Figure 10 shows the ice crystal concentrations measured with the HYVIS as a function of local temperature in clouds in comparison to the abovementioned homogeneous ice nucleation simulation. The Fletcher's (1962) ice-nucleus curve and the parameterization by Meyers et al. (1992) for contact freezing and deposition/condensation freezing are also shown for reference. In Fig. 10a, the HYVIS data from all cirrus measurements are shown; concentrations are partitioned into the 10<sup>th</sup>, 50<sup>th</sup>, and 90<sup>th</sup> percentiles. In Figs. 10b–d, the data are plotted for the lower 20% of the cloud (panel b), middle of the cloud (20% to 80% of the

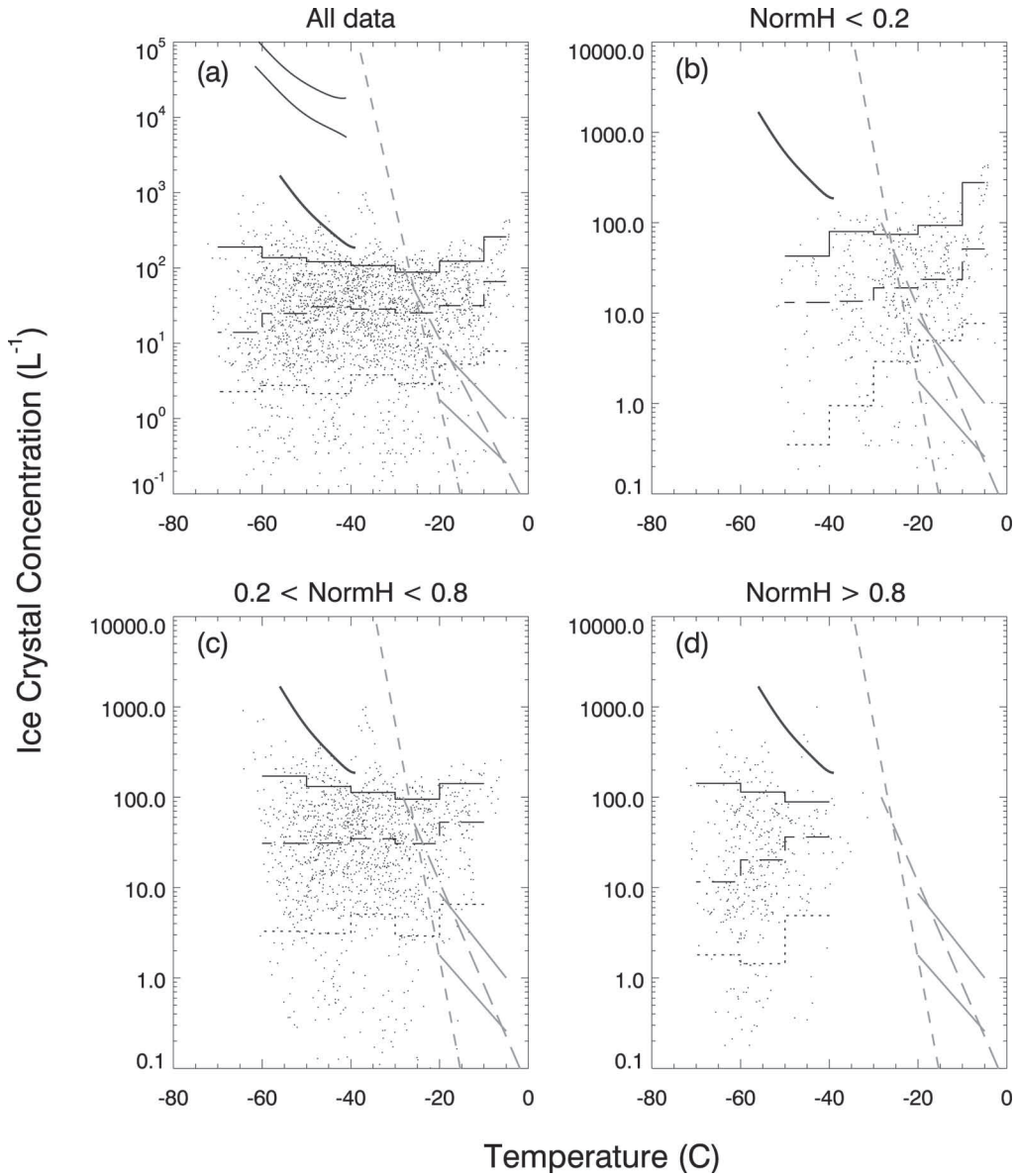


Fig. 10. Comparison between ice crystal concentrations from HYVIS observations and simulated ones from parcel cloud modeling by Heymsfield and Miloshevich (1993) as a function of in-cloud local temperature. The HYVIS data are classified according to *NormH*: (a) all data; (b) *NormH* < 0.2; (c) 0.2 < *NormH* < 0.8; (d) *NormH* > 0.8. Horizontal stepwise lines indicate the 10<sup>th</sup> (dotted), 50<sup>th</sup> (dashed), and 90<sup>th</sup> (solid) percentiles of the HYVIS measurements in order from the bottom. Three regression black curves in Fig. 10a indicate the simulated maximum concentrations of ice crystals through homogeneous ice nucleation as a function of initial parcel temperature using three different constant updraft velocities (100, 50 and 10 cm s<sup>-1</sup> from top to bottom in this panel), while only one case is indicated for the velocity of 10 cm s<sup>-1</sup> in the upper left of Figs. 10b–d. Fletcher's ice-nucleus curve (thick gray short dashed line) and Meyers' parameterizations of both contact-freezing (thick gray long dashed line) and deposition/condensation-freezing (two thick gray solid lines: 0% and -10% supersaturation with respect to water in order from the upper) are also shown in each panel for reference.



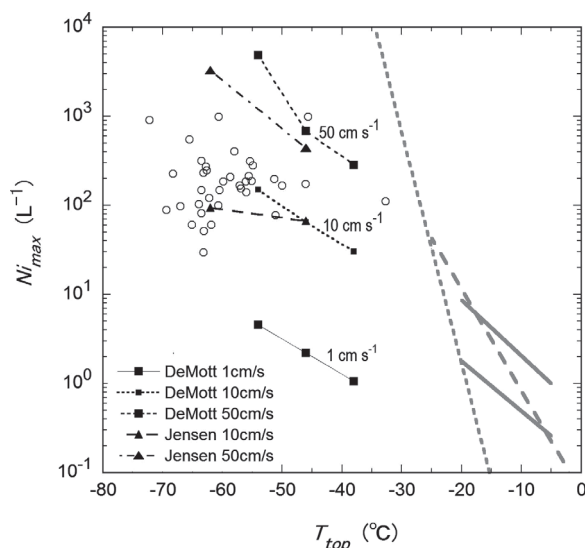


Fig. 11. Maximum ice crystal concentrations (circle) from the HYVIS measurements as a function of cloud top temperature. The square and triangle markers indicate the simulated maximum concentrations of ice crystals, cited from DeMott et al. (1997) and Jensen et al. (1997) study, respectively, through both homogeneous and heterogeneous nucleation processes as a function of updraft speed and initial parcel temperature; details are given in the text. Three constant updraft velocities of 1, 10 and  $50 \text{ cm s}^{-1}$  are denoted by different marker sizes and line types as in the legend, except for the case of  $1 \text{ cm s}^{-1}$  in the simulation by Jensen et al., and the lines between the markers are logarithmic interpolations. Other thick gray lines are also shown for reference in the same way as that shown in Fig. 10, which indicate both Fletcher's ice-nucleus curve and Meyers' parameterizations.

normalized height; panel c), and upper 20% of the cloud (panel d).

The measured ice crystal concentrations exhibited values over a wide range from the order of  $10^{-1}$  to  $10^2 \text{ L}^{-1}$ . Although it becomes critical to verify whether the simulation describes the conditions under which the HYVIS observations were made, there was a large difference between the measured concentrations and the calculated ones, even if we might expect slow updrafts ( $\sim 10 \text{ cm s}^{-1}$ ) in cirrus formation. Furthermore, the observations did not indicate a temperature dependence derived for the simulations.

However, one might expect that other physical processes besides the ice nucleation process could predominantly result in a weak temperature dependence of the ice crystal concentrations. In general, it is

difficult to separate the effect of each process on ice crystal concentrations. A complete discussion of these interpretations is beyond the scope of this study.

The comparison in Fig. 10 should be appropriate if small ice crystals are assumed to be nucleated in the vicinity of the measured levels and to dominate the total concentration. To complement the result shown in Fig. 10, Fig. 11 shows the relationship between cloud top temperature and maximum ice crystal concentration in each case of the HYVIS dataset. Similar to Fig. 10, no obvious dependence of the measured ice crystal concentrations on temperature was found. Instead of the homogeneous-only ice nucleation simulation, the simulations that focused on the combination of the homogeneous and heterogeneous ice nucleation were qualitatively compared with the HYVIS observations, as shown in Fig. 11, although our poor understanding of heterogeneous ice nucleation mechanisms could result in wide ranges in the predicted concentrations. We cite studies by Jensen and Toon (1997) and DeMott et al. (1997) on the parcel model simulations involving both ice nucleation mechanisms. Jensen and Toon (1997) used a classical model of a spherical ice cap on the insoluble particle whose efficiency as heterogeneous freezing nuclei was given by the contact angle parameter ( $m_{in}$ ). Although they assumed that  $m_{in} = 0.8$ , the results might include the uncertainties caused by very poor freezing nuclei ( $m_{in} < 0.3$ ). On the basis of the results of parcel model simulations by Jensen and Toon (1997), only the case of moderate number density ( $0.1 \text{ cm}^{-3}$ ) of soot particles acting as freezing nuclei was referred here for comparison because it could be regarded as the background value in the upper troposphere. DeMott et al. (1997) used an empirical approach defined as the effective freezing temperature ( $T^*$ ). This parameter was proposed by Sassen and Dodd (1988), and in this definition ( $T^* = T + \lambda \delta T_m$ ), the empirical coefficient ( $\lambda$ ) indicates the proportional constant for each individual solution between the freezing and equilibrium melting point depressions ( $T^* - T$ ,  $\delta T_m$ , respectively). Although no available information is relevant to CCN and IN properties in our study, we referred to the results of only the simulation assuming sulfuric acid ( $\lambda = 1$ ) as the CCN composition and unity as the number fraction of the CCN containing an insoluble component (corresponding to 10% of particle mass) given by DeMott et al. (1997). The latter assumption yields the maximum effect from heterogeneous freezing nucleation. A similar result of the predicted ice crystal concentration was reported when the CCN composition was ammonium sulfate ( $\lambda = 1.7$ ), although their simulations

suggested that the onset RH required for ice formation was significantly higher for the simulation assuming ammonium sulfate.

Although additional measurements are required to make definitive statements about ice crystal concentrations and ice nucleation processes in cirrus clouds, the qualitative comparisons shown in Figs. 10 and 11 suggest the following:

- Peak ice crystal concentrations from the homogeneous-only nucleation simulation increased steadily from  $-40^{\circ}$  to  $-60^{\circ}\text{C}$ . In contrast, there was no discernable increase in the concentrations with decreasing temperature, even near the cloud top where most ice crystals were likely to be nucleated at adjacent heights and less affected through different heights (compared to other locations) by other microphysical and dynamical processes; concentrations were either flat or lower with decreasing temperature.
- The HYVIS measurements appeared to be closer to the lower concentration involving the heterogeneous nucleation simulations for the same magnitude of updraft velocity. As indicated by the homogeneous and heterogeneous nucleation simulation via the Jensen et al. scheme, the predicted concentration had a weaker dependence on temperature for the simulation with weaker updraft velocity ( $10\text{ cm s}^{-1}$ ), which agrees better with the measured temperature dependence.

The above statements on implications of the HYVIS measurements are applicable even to mineral dust, which is one of the most dominant natural compositions among different types of aerosols for heterogeneous ice nucleation. Eidhammer et al. (2009) conducted an intercomparison of three different heterogeneous ice nucleation parameterizations proposed by previous studies focusing on the immersion or condensation freezing modes. Figures 3 and 4 in their study show the dependence of ice crystal concentrations predicted by the parcel model on vertical velocity and initial dust number concentrations. The initial temperatures (pressures) were  $-14^{\circ}$  (800 hPa) and  $-40^{\circ}\text{C}$  (340 hPa), respectively, and the details on the parcel model simulations were described in their paper. Even in regions of high dust concentrations (where heterogeneous ice nucleation is dominant), the three parameterizations differ in the predicted ice crystal concentrations by a factor of about 2 to 10 in the vertical velocity range below  $50\text{ cm s}^{-1}$  owing to freezing onset conditions and rates. However, within the same parameterization, the dependence of ice crystal concentrations on temperature or vertical velocity in

case of dust particles is deemed to involve the same qualitative feature as the other cases in Fig. 11. The HYVIS measurements tend to be closer to the lower predicted concentrations of ice crystals in the heterogeneous nucleation regime, although the dependence on initial dust concentrations differs significantly among the three parameterizations.

As noted in Section 2, the HYVIS measurements enabled us to acquire reliable size distributions of ice crystals above  $30\text{ }\mu\text{m}$  or perhaps even smaller. Because we conclude that the measurements presented herein, although less accurate, do not substantially underestimate the total concentration in the observed cirrus clouds even when adding our  $10\text{--}30\text{ }\mu\text{m}$  concentrations, we infer that the heterogeneous ice nucleation process is important (or even dominates) for the type of cirrus studied here, namely synoptically-generated cirrus. Research will be needed to further investigate the details of the relationship between the ice crystal concentration and ice nucleation processes active in cirrus clouds.

To infer whether our data suggest that heterogeneous ice nucleation is the dominant process, other recent field observations could be used to support our results. DeMott et al. (2010) showed that their measured IN number concentrations from nine field programs had a remarkable correlation with those of aerosol particles larger than  $0.5\text{ }\mu\text{m}$ . In the mentioned study, the observed range of IN concentrations was restricted to temperatures above  $-35^{\circ}\text{C}$ , where homogeneous nucleation (freezing) does not occur. The similarity between these concentrations and our results suggest that the ice crystals in our study were predominantly formed by heterogeneous nucleation. We cannot rule out the possibility that within cirrus clouds or in cirrus forming regions, there are localized regions where homogeneous ice nucleation occurs sporadically; when this occurs, relative humidities drop rapidly to prevent further homogeneous nucleation.

## 5. Summary and conclusions

This study reports on ice crystal concentrations measured in synoptically-generated cirrus clouds by a balloonborne videosonde, which has the advantage of more reliably measuring small ice crystals in the size range of  $10\text{--}100\text{ }\mu\text{m}$  than the conventional aircraft instruments. We have collected a unique dataset of cirrus ice particle concentrations from nearly 40 launches of the HYVIS. The comparison tests between the HYVIS and other airborne microphysical instruments, conducted in the laboratory, suggested that the CE of the HYVIS had an uncertainty factor of 2–3 for

10–30  $\mu\text{m}$  particles and less than 2 for particles larger than 30  $\mu\text{m}$ . From the degree of uncertainty in the *CE* of the HYVIS, the observed broad size distributions of ice crystals, and low ice-supersaturation conditions, we conclude that the measurements presented in this study do not substantially underestimate the total concentration, although there exists some uncertainty about the concentration measurements at particle sizes smaller than 30  $\mu\text{m}$ .

The focus of this study was to report on the concentrations of ice crystals in cirrus as they relate to cloud radiation. The vertical distributions of the ice crystal concentrations were found to be roughly constant, except for those near the cloud top and base. Although the maximum concentrations were located mostly ( $\sim 35\%$ ) near the cloud top ( $\text{Norm}H \geq 0.8$ ) among five equally partitioned cloud layers, they occurred at various vertical locations; there was no correlation between the cloud depth and the normalized height or the distance from the cloud top, where the maximum concentrations occurred. Typical concentrations were of the order of 10 to 100  $\text{L}^{-1}$ . The relative humidity profiles in the vertical combined with the associated frequency of occurrence of the various crystal habits, suggest that sublimation should be responsible for the observed increase in the frequency of single bullets near the cloud base and there was an enhancement in the concentrations near the cloud base in some cases.

A comparison between ice crystal concentrations measured with the HYVIS and simulated with parcel cloud models has helped in the interpretation of the ice nucleation mechanisms in these cirrus clouds. From this comparison, homogeneous ice nucleation produces concentrations of the order of 1 to 10  $\text{cm}^{-3}$ , which is significantly higher than our measured result and strongly dependent on temperature. It was noteworthy that the concentration measurements did not indicate such strong dependence on temperature, even near the cloud top where many ice crystals were supposed to be nucleated. The results suggest that various physical processes are involved in the vertical profile of ice crystal concentrations; the concentration decreases owing to ice crystal growth and its fallout; on the other hand, it increases owing to heterogeneous ice nucleation and/or ice particle breakup.

In the parcel model simulations presented here and perhaps in clouds, the homogeneous ice nucleation process ceases shortly after the peak RH is attained. The size distribution should then shift to larger sizes in response to ice crystal growth and fallout producing a narrow size distribution, in which the concentration

falls off rapidly at small sizes. Thereafter, additional crystals may be produced by heterogeneous nucleation or a type of breakup mechanism, leading to a broad size distribution. Because we often observed broad size distributions (at least down to 10  $\mu\text{m}$ ), the heterogeneous nucleation process or a breakup mechanism is necessary to explain the observations.

However, there are several uncertainties that make it difficult to conclude whether homogeneous or heterogeneous ice nucleation was the dominant mechanism operated in the clouds under study. First, the concentrations of ice crystals nucleated by homogeneous nucleation are critically dependent on the updraft velocity, and we are not aware of the values of vertical velocity in the observed clouds. Second, substantial uncertainties are included in numerical simulations of cirrus formation through the homogeneous nucleation process, as suggested by early studies. Moreover, there were no measured data in the clouds under study suggesting any information of primary importance about the cirrus initiation processes, such as physical and chemical properties of aerosols (serving as CCN and IN), peak relative humidity, and updraft velocity. These data will be highly useful for further understanding the cirrus formation mechanisms. With these desired datasets, recent modeling and laboratory studies would also greatly help to interpret in situ microphysical measurements of cirrus clouds.

### Acknowledgments

We wish to thank the staff of the JMA TATENO Aerological Observatory and Mr. H. Mizuno, Dr. Y. Yamada, Ms. M. Hoshimoto, and the Cloud Physics Laboratory staff of the M.R.I. for their cooperation in the HYVIS observations. The JACCS program was supported by the Science and Technology Agency of Japanese Government. We would also like to thank the reviewers for their constructive and helpful comments.

### Appendix: Comparison between HYVIS and other instruments

The HYVIS captures images of the hydrometeors whose sizes are larger than 10- $\mu\text{m}$  diameter. For water droplets, there was a relatively sharp increase in the collection efficiency (*CE*) of the HYVIS at diameters between 10 and 20  $\mu\text{m}$  compared to the FSSP measurements in an artificial fog of droplets smaller than 100  $\mu\text{m}$  in our laboratory. The *CE* was considered to reach unity before the droplet size increased to 20  $\mu\text{m}$ . For sampling of ice particles, the actual *CE* should be confirmed and evaluated, which is dominantly

influenced by stickiness of a collecting surface coated with silicone oil.

Unfortunately, neither standardized instruments nor techniques are recognized for measuring concentrations of small ice particles ( $< 100 \mu\text{m}$ ). The HYVIS measurements were compared with the SPEC CPI (version 2) measurements as a reference for ice crystals formed in our laboratory. Ice fog was artificially prepared in a cold room by glaciating supercooled fog with a small piece of dry ice. The size of ice particles ranged from several microns to  $100\text{--}200 \mu\text{m}$ . To minimize the uncertainty of the sample area of the CPI, a cylindrical sample nozzle with an inner diameter of 2 mm was attached to the inlet in such a way that the nozzle axis was aligned with respect to the optical center of the CPI's particle detection system.

The ratio of particle number concentrations measured with the HYVIS and CPI increased with size in the range of  $10\text{--}30 \mu\text{m}$ ; the average value of the ratio increased from about 0.5 to 1.5 (with deviation from 0.3 to 3) over the size range. We also found that the actual *CE* of the HYVIS for ice crystals larger than  $30 \mu\text{m}$  agreed with the theoretical estimate within an uncertainty factor of 2. However, further experiments (with a more reliable instrument and technique) are needed for quantitative estimation of the *CE* in the size range of  $10\text{--}30 \mu\text{m}$ .

The HYVIS would greatly underestimate ice crystal concentrations when it is used for measuring cirrus clouds where ice germs smaller than  $10 \mu\text{m}$  are dominantly present, for example, some anvils or cirrus clouds at an early stage of their life cycle. As shown in Fig. 2, the size distributions in the HYVIS dataset were not extremely steep at sizes smaller than  $30 \mu\text{m}$ . This feature would be responsible for little difference between total concentrations including and excluding particles in the size range of  $10\text{--}30 \mu\text{m}$  in Fig. 3. Thus, we believe that the uncertainty of the *CE* should have a rather small impact on the total concentrations of ice crystals larger than  $10 \mu\text{m}$  for the dataset presented in this study because the *CE* of the HYVIS over this size range does not change by more than a factor of 2.

## References

- Asano, S., and JACCS Cirrus Observation Team, 1997: A sonde system for simultaneous measurements of radiative and cirrus microphysics in the Japanese Cloud-Climate Study (JACCS) program. *IRS'96: Current Problems in Atmospheric Radiation*, Smyth, W. L., and K. Stamnes (eds.), Deepak Publishing, 349–352.
- Baumgardner, D., and Coauthors, 2012: In situ, airborne instrumentation: Addressing and solving measurement problems in ice clouds. *Bull. Amer. Meteor. Soc.*, **93**, ES29–ES34.
- Connolly, P. J., M. J. Flynn, Z. Ulanowski, T. W. Choularton, M. W. Gallagher, and K. N. Bower, 2007: Calibration of the cloud particle imager probes using calibration beads and ice crystal analogs: the depth of field. *J. Atmos. Oceanic Technol.*, **24**, 1860–1879.
- DeMott, P. J., 2002: Laboratory studies of cirrus cloud processes. *Cirrus*, Lynch, D. K., K. Sassen, D. O'C. Starr, and G. Stephens (eds.), Oxford University Press, 102–135.
- DeMott, P. J., 2007: Progress and issues in quantifying ice nucleation involving atmospheric aerosols. *Nucleation and Atmospheric Aerosols*, O'Dowd, C. D., and P. E. Wagner (eds.), Springer, 405–417.
- DeMott, P. J., M. P. Meyers, and W. R. Cotton, 1994: Parameterization and impact of ice initiation processes relevant to numerical model simulations of cirrus clouds. *J. Atmos. Sci.*, **51**, 77–90.
- DeMott, P. J., D. C. Rogers, and S. M. Kreidenweis, 1997: The susceptibility of ice formation in upper tropospheric clouds to insoluble aerosol components. *J. Geophys. Res.*, **102**, 19575–19584.
- DeMott, P. J., and Coauthors, 2010: Predicting global atmospheric ice nuclei distributions and their impacts on climate. *Proc. Natl. Acad. Sci., USA*, **107**, 11217–11222, doi:10.1073/pnas.0910818107.
- Dong, Y., R. G. Oraltay, and J. Hallett, 1994: Ice particle generation during evaporation. *Atmos. Res.*, **32**, 45–53.
- Dowling, D. R., and L. F. Radke, 1990: A summary of the physical properties of cirrus clouds. *J. Appl. Meteor.*, **29**, 970–978.
- Eidhammer, T., P. J. DeMott, and S. M. Kreidenweis, 2009: A comparison of heterogeneous ice nucleation parameterizations using a parcel model framework. *J. Geophys. Res.*, **114**, D06202, doi:10.1029/2008JD011095.
- Field, P. R., R. Wood, P. R. A. Brown, P. H. Kaye, E. Hirst, R. Greenaway, and J. A. Smith, 2003: Ice particle interarrival times measured with a Fast FSSP. *J. Atmos. Oceanic Technol.*, **20**, 249–261.
- Field, P. R., A. J. Heymsfield, and A. Bansemer, 2006: Shattering and particle interarrival times measured by optical array probes in ice clouds. *J. Atmos. Oceanic Technol.*, **23**, 1357–1370.
- Fletcher, N. H., 1962: *Physics of Rain Clouds*. Cambridge University Press, 386pp.
- Fukuta, N., and L. A. Walter, 1970: Kinetics of hydrometeor growth from a vapor-spherical model. *J. Atmos. Sci.*, **27**, 1160–1172.
- Gardiner, B. A., and J. Hallett, 1985: Degradation of in-cloud forward scattering spectrometer probe measurements in the presence of ice particles. *J. Atmos. Oceanic Technol.*, **2**, 171–180.
- Gayet, J.-F., G. Febvre, and H. Larsen, 1996: The reliability of the PMS FSSP in the presence of small ice crystals. *J. Atmos. Oceanic Technol.*, **13**, 1300–1310.



- Gierens, K., 2003: On the transition between heterogeneous and homogeneous freezing. *Atmos. Chem. Phys.*, **3**, 437–446.
- Gierens, K., M. Monier, and J.-F. Gayet, 2003: The deposition coefficient and its role for cirrus clouds. *J. Geophys. Res.*, **108**, 4069, doi:10.1029/2001JD001558.
- Gow, A. J., 1965: On the origin of bullet crystals at the South Pole. *J. Glaciol.*, **16**, 461–465.
- Hallett, J., 1976: Measurements of size, concentration and structure of atmospheric particulates by the airborne continuous particle replicator. Air Force Geophysics Laboratory Tech. Rep., AFGL-TR-76-0149, 151pp.
- Heymsfield, A. J., and C. M. R. Platt, 1984: A parameterization of the particle size spectrum of ice clouds in terms of the ambient temperature and ice water content. *J. Atmos. Sci.*, **41**, 846–855.
- Heymsfield, A. J., and R. M. Sabin, 1989: Cirrus crystal nucleation by homogeneous freezing of solution droplets. *J. Atmos. Sci.*, **46**, 2252–2264.
- Heymsfield, A. J., and L. M. Miloshevich, 1993: Homogeneous ice nucleation and supercooled liquid water in orographic wave clouds. *J. Atmos. Sci.*, **50**, 2335–2353.
- Heymsfield, A. J., and L. M. Miloshevich, 1995: Relative humidity and temperature influences on cirrus formation and evolution: Observations from wave clouds and FIRE II. *J. Atmos. Sci.*, **52**, 4302–4326.
- Heymsfield, A. J., and G. M. McFarquhar, 1996: High albedos of cirrus in the tropical Pacific warm pool: Microphysical interpretations from CEPEX and from Kwajalein, Marshall Islands. *J. Atmos. Sci.*, **53**, 2424–2451.
- Ivanova, D., D. L. Mitchell, W. P. Arnott, and M. Poellot, 2001: A GCM parameterization for bimodal size spectra and ice mass removal rates in mid-latitude cirrus clouds. *Atmos. Res.*, **59–60**, 89–113.
- Jensen, E. J., and O. B. Toon, 1997: The potential impact of soot particles from aircraft exhaust on cirrus clouds. *Geophys. Res. Lett.*, **24**, 249–252.
- Jensen, E. J., and Coauthors, 1998: Ice nucleation processes in upper tropospheric wave-clouds observed during SUCCESS. *Geophys. Res. Lett.*, **25**, 1363–1366.
- Korolev, A. V., E. F. Emery, J. W. Strapp, S. G. Cober, G. A. Isaac, M. Wasey, and D. Marcotte, 2011: Small ice particles in tropospheric clouds: fact or artifact? Airborne Icing Instrumentation Evaluation Experiment. *Bull. Amer. Meteor. Soc.*, **92**, 967–973.
- Lawson, R. P., 2011: Effects of ice particles shattering on the 2D-S probe. *Atmos. Meas. Tech.*, **4**, 1361–1381.
- Lawson, R. P., A. J. Heymsfield, S. M. Aulenbach, and T. L. Jensen, 1998a: Shapes, sizes and light scattering properties of ice crystals in cirrus and a persistent contrail during SUCCESS. *Geophys. Res. Lett.*, **25**, 1331–1334.
- Lawson, R. P., A. V. Korolev, S. G. Cober, T. Huang, J. W. Strapp, and G. A. Isaac, 1998b: Improved measurements of the drop size distribution of a freezing drizzle event. *Atmos. Res.*, **47–48**, 181–191.
- Lawson, R. P., B. A. Baker, C. G. Schmitt, and T. L. Jensen, 2001: An overview of microphysical properties of Arctic clouds observed in May and July 1998 during FIRE ACE. *J. Geophys. Res.*, **106**, 14989–15014.
- Lawson, R. P., D. O'Connor, P. Zmarzly, K. Weaver, B. A. Baker, Q. Mo, and H. Jonsson, 2006: The 2D-S (Stereo) probe: design and preliminary tests of a new airborne, high-speed, high-resolution particle imaging probe. *J. Atmos. Oceanic Technol.*, **23**, 1462–1477.
- Lin, R.-F., D. O'C. Starr, P. J. DeMott, R. Cotton, K. Sassen, E. Jensen, B. Kärcher, and X. Liu, 2002: Cirrus parcel model comparison project. Phase 1: The critical components to simulate cirrus initiation explicitly. *J. Atmos. Sci.*, **59**, 2305–2329.
- Liou, K. N., 1986: Influence of cirrus clouds on weather and climate processes: A global perspective. *Mon. Wea. Rev.*, **114**, 1167–1199.
- Magee, N., A. M. Moyle, and D. Lamb, 2006: Experimental determination of the deposition coefficient of small cirrus-like ice crystals near  $-50^{\circ}\text{C}$ . *Geophys. Res. Lett.*, **33**, L17813, doi:10.1029/2006GL026665.
- Meyers, M. P., P. J. DeMott, and W. R. Cotton, 1992: New primary ice nucleation parameterizations in an explicit cloud model. *J. Appl. Meteor.*, **31**, 708–721.
- Miloshevich, L. M., and A. J. Heymsfield, 1997: A balloon-borne continuous cloud particle replicator for measuring vertical profiles of cloud microphysical properties: Instrument design, performance, and collection efficiency analysis. *J. Atmos. Oceanic Technol.*, **14**, 753–768.
- Miloshevich, L. M., H. Vömel, A. Paukkunen, A. J. Heymsfield, and S. J. Oltmans, 2001: Characterization and correction of relative humidity measurements from Vaisala RS80-A radiosondes at cold temperatures. *J. Atmos. Oceanic Technol.*, **18**, 135–156.
- Mishchenko, M. I., W. B. Rossow, A. Macke, and A. A. Lacis, 1996: Sensitivity of cirrus cloud albedo, bidirectional reflectance and optical thickness retrieval accuracy to ice particle shape. *J. Geophys. Res.*, **101**, 16973–16985.
- Murakami, M., and T. Matsuo, 1990: Development of the hydrometeor videosonde. *J. Atmos. Oceanic Technol.*, **7**, 613–620.
- Orikasa, N., and M. Murakami, 1997: A new version of hydrometeor videosonde for cirrus cloud observations. *J. Meteor. Soc. Japan*, **75**, 1033–1039.
- Ranz, W. E., and J. B. Wong, 1952: Impaction of dust and smoke particles on surface and body collectors. *Ind. Eng. Chem.*, **44**, 1371–1381.
- Sassen, K., and G. C. Dodd, 1988: Homogeneous nucleation rate for highly supercooled cirrus cloud droplets. *J. Atmos. Sci.*, **45**, 1357–1369.
- Sassen, K., and G. C. Dodd, 1989: Haze particle nucleation simulations in cirrus clouds, and applications for numerical modeling and lidar studies. *J. Atmos. Sci.*, **46**, 3005–3014.
- Sassen, K., and J. R. Campbell, 2001: A midlatitude cirrus cloud climatology from the facility for atmospheric



- remote sensing. Part I: Macrophysical and synoptic properties. *J. Atmos. Sci.*, **58**, 481–496.
- Schmitt, C. G., and W. P. Arnott, 1999: Infrared emission (500–2000  $\text{cm}^{-1}$ ) of laboratory ice clouds. *J. Quant. Spectros. Radiat. Transfer*, **63**, 701–725.
- Schmitt, C. G., and A. J. Heymsfield, 2009: The size distribution and mass-weighted terminal velocity of low-latitude tropopause cirrus crystal populations. *J. Atmos. Sci.*, **66**, 2013–2028.
- Spichtinger, P., and K. M. Gierens, 2009: Modelling of cirrus clouds—Part 2: Competition of different nucleation mechanisms. *Atmos. Chem. Phys.*, **9**, 2319–2334.
- Stephens, G. L., S. C. Tsay, P. W. Stackhouse, Jr., and P. J. Flatau, 1990: The relevance of the microphysical and radiative properties of cirrus clouds to climate and climatic feedback. *J. Atmos. Sci.*, **47**, 1742–1753.
- Strapp, J. W., F. Albers, A. Reuter, A. V. Korolev, U. Maixner, E. Rashke, and Z. Vukovic, 2001: Laboratory measurements of the response of a PMS OAP-2DC. *J. Atmos. Oceanic Technol.*, **18**, 1150–1170.
- World Meteorological Organization (WMO), 1975: *International Cloud Atlas, vol. 1, Manual on the Observation of Clouds and Other Meteors*, WMO No. 407, WMO, Geneva, 155pp.